Bulletin of Earthquake Engineering (2023) 21:2785–2815
https://doi.org/10.1007/s10518-023-01632-y

ORIGINAL ARTICLE

# Experimental study of high-strength steel fiber concrete exterior beam-column joints with high-strength steel reinforcements

**Jianxin Zhang[1,2] · Xiaoxue Zhao[1] · Xian Rong[1,2] · Yanyan Li[1,2]**

Received: 14 January 2022 / Accepted: 24 January 2023 / Published online: 4 February 2023


**Abstract**
This study aims to evaluate the seismic performance of exterior beam-column joints (BCJs) having high-strength steel (HSS) reinforcements in beams and columns coupled with high-strength steel fiber reinforced concrete (HSSFRC). Eight full-scale exterior BCJs with various reinforcement detailing were designed for a moment-resisting frame and subjected to reversed cyclic loading. The parameters in the test include reinforcement strength, concreting pattern in different regions and shear compressive ratio. The amounts of HSS reinforcements in beams, with a yield strength of 600 MPa, were reduced by 22.6% for specimens SEJH1 and EJH1 with 9% higher flexural strength and by 33.3% for the other specimens with 6% lower flexural strength, respectively, due to the enhancement in yield strength. The joints reinforced with HSS reinforcement showed similar failure modes, energy dissipation and secant stiffness as the specimens using 400 MPa reinforcement. Substitution of 400 MPa bars with a smaller amount of 600 MPa as beam longitudinal reinforcements was favorable to seismic performance and could resolve reinforcement congestion. While using HSSFRC effectively enhanced the ductility, decreased slippage of beam longitudinal reinforcements, improved concrete crushing and decreased shear deformation in the joint core due to improved bond degradation of HSS bars; but the peak load and secant stiffness were not significantly affected. The analytical results of design codes in GB50010 were agreed with the experimental results.

**Keywords** Beam-column joints · Seismic performance · High-strength steel · Steel fiber · Ductility

✉ Jianxin Zhang
zhangjianxin505@hebut.edu.cn

[1] School of Civil and Transportation Engineering, Hebei University of Technology, Tianjin 300401, China

[2] Civil Engineering Technology Research Center of Hebei Province, Hebei University of Technology, Tianjin 300401, China

## 1 Introduction

Beam-column joints that transfer loads between beams and columns are key parts in structures to resist earthquake loads (Kotsovou and Mouzakis 2012). The failure of joints may lead to large story drifts, even the collapse of structures due to inadequate ductility (Tapan et al. 2013). Under the seismic action, the joint is usually subjected to the greater shear action which will lead to failure, so the joint must have a higher deformation ability and ductility (Chetchotisak et al. 2020; Favvata and Karayannis 2014; Zainal et al. 2021). Excessive reinforcement requirements in beam-column joints (BCJs) may lead to reinforcement congestion at the joint core area, resulting in the difficulty of concrete pouring and construction (Guan et al. 2019). Moreover, RC moment frames often required large section sizes. Using high-strength steel (HSS) reinforcements is a way to alleviate reinforcement congestion by effectively reducing the amount of steel bars when compared to normal-strength materials (Rautenberg et al. 2013; Su et al. 2021). In addition to using HSS, the application of appropriate splice method also could eliminate bar congestion in beams, columns or joints' core. (Dabiri and Kheyroddin 2021; Eddy and Nagai 2016; Chun et al. 2009). Adding steel fibers into high-strength concrete could mitigate the above issues by enhancing toughness and deformation ability. Kang et al. (2019) designed three reinforced concrete beam-column joints under cyclic loading. Results showed that beam-column joints with HSS bars could bear great lateral displacement and had high behavior. And the joints reinforced with steel fibers reduced the amount of steel bars.

Recently, scholars have been devoted to research the seismic performance of beam-column joints with HSS bars (Alaee and Li 2017a; Feng et al. 2020; Kim and Chang 2021). Hwang et al. (2014) studied the use of 600 MPa steel bars as beam bending steel bars to study the seismic performance of four interior joints and three exterior joints under cyclic lateral loads. Chang et al. (2014) experimentally studied the seismic performance of ordinary concrete beam-column joints with 690 MPa reinforcements and the effectiveness of using HSS bars was evaluated. Alavi-Dehkordi et al. (2019) studied the effect of 600 MPa HSS bars with high-strength concrete on the seismic behavior of six exterior beam-column joints subjected to quasi-static reversed cyclic loading. Alaee and Li (2017b) studied the seismic behavior of five reinforced concrete exterior beam-column joints with 500 MPa and 700 MPa strength bars. Results showed that the joints with 700 MPa bars had smaller energy dissipation capacity, and the beam steel bars were more prone to slip as well as had lower bond strength.

HSS bars can potentially enhance the load capacity of a beam-column joint while effectively reducing the amount of required steel bars, alleviate reinforcement congestion, address high shear demand, and ensure the construction quality. But the bond strength of HSS bars is lower than that of ordinary steel bars, so it is prone to bond-slip under reversed cyclic loading. However, using HSS bars is restricted for RC beam-column joints due to upper limits of steel strength, which are differed in various codes and recommendations. ACI 318-14 (2014) limits the strength of flexural and shear reinforcements up to 420 MPa. In EC8 (2004) and GB 50010 (2015), the strength of longitudinal reinforcements is limited to 500 MPa. To extend the extreme values of steel bars, with the yield strength of over 500 MPa, updated guidelines are necessary for design of the RC moment frame. The seismic performance of beam-column joints with HSS bars is need further studied.

High-strength concrete (HSC) can alleviate the brittleness defects and restrict the early slip of reinforcements at the joint regions when HSS bars are used. Ehsani et al. (1987) reported the behavior of four beam-column joints with HSC subjected to cyclic loading.

Ashtiani et al. (2014) studied the effect of HSC on the bond behavior of interior beam-column assemblies. Ahmed et al. (2019) experimentally studied the ductility of beam-column joints with HSC. These research results showed that the beam-column joints with HSC could bear a better seismic capacity compared with ordinary concrete.

Steel fiber reinforced concrete (SFRC) is made by adding steel fiber into concrete, which can inhibit the development of flexural and shear cracks. Compared with ordinary concrete, SFRC has better ductility, energy dissipation capacity and bonding performance (Khan et al. 2018; Raj et al. 2020). Tang et al. (1992) introduced the test results of SFRC beam-column joints under cyclic loading. Test results showed that the shear strength of BCJs with SFRC was significantly improved. Kheni et al. (2015) and Ghani and Hami (2013) reported that the use of hybrid fiber-reinforced concrete in BCJs improved displacement ductility and energy dissipation capacity. Saghafi and Shariatmadar (2018) introduced high performance fiber reinforced cement-based composites with 2% steel fiber used in beam-column joints, and the mechanical properties of all specimens were improved. According to the existing literatures, steel fiber can improve the ductility of concrete, increase the bond performance and improve the seismic performance of BCJs with ordinary-strength steel bars. When the HSS bars are used, the stress level of the reinforcements is different.

Ordinary-strength steel bars coupled with SFRC have been used in BCJs, which showed better seismic performance. However, the effect of high strength steel fiber reinforced concrete (HSSFRC) coupled with HSS bars on seismic behavior of beam-column joints had not been determined, which needs further study. And the reasonable application range of HSSFRC should be also further studied. In addition, there are more researches on the interior BCJs at present, and fewer researches on the exterior BCJs, which had much more reinforcements in the joint area resulting in steel bar congestion.

This study presents a study on the seismic behavior of eight exterior BCJs strengthened with HSS bars and HSSFRC, and aims to verify the effectiveness of HSS bars coupled with HSSFRC to alleviate reinforcement congestion and enhance ductility. The parameters included the reinforcement strength, concreting pattern in different regions and shear compressive ratio. The seismic performance was studied in terms of failure mode, stiffness, strength and energy dissipation. And failure mode and strength were predicted in accordance with the design code in GB 50010.

## 2 Experimental program

### 2.1 Description of specimens

In view of the complex stress of reinforced concrete frame joints, which are prone to be damaged in the earthquake, eight reinforced concrete exterior BCJs with the same size but different reinforcement details were designed in this study. These specimens simulated the exterior BCJs of a four-story RC moment-resisting frame structure were labeled as EJH1, EJH2, EJN1, SEJH1, SEJH2, SEJH3, SEJH4 and SEJH5, respectively. The letter “EJ” stands for the exterior type of beam-column joints. The letter “H”, “N” and “S” indicate specimens with HSS bars, ordinary steel bars and HSSFRC, respectively. The influences of reinforcement strength, concrete type, and shear compression ratio on the seismic performance of exterior BCJs were studied. The ratios of the column to beam moment capacity were 2.56 for EJN1, 3.24 for specimens EJH1 and

SEJH1, and 2.78 for the other joints, which was higher than the requirements of the strong column-weak beam in accordance with the code of GB 50010.

Specimen EJN1, as a reference joint, was produced with HSC and ordinary-strength steel bars (yield strength = 400 MPa) and intended to shear failure in the joint to ensure strength and stiffness. Eighteen deformed 18-mm steel bars were arranged as the longitudinal reinforcements in the beams, and six deformed 25-mm steel bars and two 20-mm steel bars (yield strength = 400 MPa) were used as the longitudinal reinforcements in the columns. For specimens EJH1 and EJH2 with 22.6% and 33.3% lower beam reinforcement ratio of HRB600 when compared with joint EJN1, with the principle of reductions proportional to the enhancements achieved in yield stress, the substitution of HSS reinforcements for ordinary-strength steel bars was fabricated as longitudinal reinforcements in the beams and columns. Fourteen and twelve deformed 18-mm steel bars with a yield strength of 600 MPa were used in the beams of EJH1 and EJH2, respectively. The difference in EJH1 and EJH2 was the shear compression ratio, which was equal to shear force divided by concrete compression strength and sectional area, and the values were 0.244 and 0.209, respectively. In the case of specimens SEJH1 and SEJH2, HSC was replaced by HSSFRC with 1.2% volume ratio in the joint core, beams and columns. The other details of SEJH1 and SEJH2 were the same as that of EJH1 and EJH2, respectively. There were three concreting patterns with HSSFRC for specimens SEJH3, SEJH4 and SEJH5: only in the joint core region for specimen SEJH3, joint core region and beam end at 350 mm for joint SEJH4, and core region and beam end at 550 mm for specimen SEJH5, the other parts were poured with HSC. Six deformed bars with a diameter of 25 mm and two deformed bars with a diameter of 20 mm, with the yield strength of 600 MPa, were used as the longitudinal bars of the column except for joint EJN1. Seven stirrups with a diameter of 10 mm were placed in the joint region, and deformed 10-mm steel bars with the spacing of 100 mm were used as transverse reinforcement in the beams and columns for all specimens. The column section was 350 mm × 350 mm and the height of 2800 mm, the beam section was 250 mm × 400 mm and the length of 1600 mm. The details of all specimens are shown in Tables 1, 2 and Fig. 1.

**Table 1** Details of test specimens

| Specimens | SRC | Concreting pattern | HSSFRC region | Reinforcement strength |
|---|---|---|---|---|
| EJH1 | 0.244 | HSC | – | HRB600 |
| EJH2 | 0.209 | HSC | – | HRB600 |
| EJN1 | 0.217 | HSC | – | HRB400 |
| SEJH1 | 0.244 | HSSFRC | Joint core & beam & column | HRB600 |
| SEJH2 | 0.209 | HSSFRC | Joint core & beam & column | HRB600 |
| SEJH3 | 0.209 | HSSFRC & HSC | Joint core | HRB600 |
| SEJH4 | 0.209 | HSSFRC & HSC | Joint core & 350 mm beam end | HRB600 |
| SEJH5 | 0.209 | HSSFRC& HSC | Joint core & 550 mm beam end | HRB600 |

SRC, shear compressive ratio; –, without this parameter

**Table 2** Property of test specimens

| Member | Property | EJH1 | EJH2 | EJN1 | SEJH1 | SEJH2 | SEJH3 | SEJH4 | SEJH5 |
|---|---|---|---|---|---|---|---|---|---|
| Beam | Dimensions (mm) | 250×400 | | | | | | | |
| | Top bar area ratio (%) | 1.78 | 1.53 | 2.29 | 1.78 | 1.53 | 1.53 | 1.53 | 1.53 |
| | Bottom bar area ratio (%) | 1.78 | 1.53 | 2.29 | 1.78 | 1.53 | 1.53 | 1.53 | 1.53 |
| | Longitudinal bars grade (MPa) | 600 | 600 | 400 | 600 | 600 | 600 | 600 | 600 |
| | Longitudinal bars size (mm) | 18 | 18 | 18 | 18 | 18 | 18 | 18 | 18 |
| | Moment capacity (kN·m) | 249.1 | 213.6 | 221.8 | 249.1 | 213.6 | 213.6 | 213.6 | 213.6 |
| Column | Dimensions (mm) | 350×350 | | | | | | | |
| | Bar area ratio (%) | 2.62 | 2.62 | 2.62 | 2.62 | 2.62 | 2.62 | 2.62 | 2.62 |
| | Corner bar grade (MPa) | 600 | 600 | 400 | 600 | 600 | 600 | 600 | 600 |
| | Corner bar size (mm) | 25 | 25 | 25 | 25 | 25 | 25 | 25 | 25 |
| | Middle bar grade (MPa) | 400 | 400 | 400 | 400 | 400 | 400 | 400 | 400 |
| | Middle bar size (mm) | 20 | 20 | 20 | 20 | 20 | 20 | 20 | 20 |
| | Axial load ratio | 0.15 | 0.15 | 0.15 | 0.15 | 0.15 | 0.15 | 0.15 | 0.15 |
| | Nominal flexural moment (kN·m) | 346.0 | 346.0 | 283.31 | 346.0 | 346.0 | 346.0 | 346.0 | 346.0 |
| | Ratio of column-to-beam moment | 2.78 | 3.24 | 2.56 | 2.78 | 3.24 | 3.24 | 3.24 | 3.24 |
| Joint | Stirrup diameter (mm) | 10 | 10 | 10 | 10 | 10 | 10 | 10 | 10 |
| | Stirrup grade (MPa) | 400 | 400 | 400 | 400 | 400 | 400 | 400 | 400 |

## 2.2 Materials

The concrete used in this test was HSC and HSSFRC. HSC was adopted grade C55 strength commercial concrete, and the concrete cover was 25 mm. In order to ensure that the concrete vibrated and compacted when pouring, concrete poured in the core area of the joint was first, and then other parts of the concrete was poured. HSSFRC was made by adding hook shear steel fiber with 1.2% volume percentage to the HSC. The length of steel fiber was 30 mm and the tensile strength was about 1000 MPa. A group of cubic specimens with the side length of 150 mm and dumbbell-shaped specimens with the diameter of 100 mm at the middle section were made and the corresponding compressive and tensile tests were conducted after a curing period of 28 days. The load-controlled method was adopted for compressive and tensile tests, and the loading speed was 0.5–0.8 MPa/s under compressive and 0.08–0.10 MPa/s under tensile in accordance with GB/T 50081-2019 (2019). The mechanical performance of concrete is shown in Table 3.

Four-point-bending tests were also conducted on prismatic specimens BS1-BS6 of dimensions 100 mm × 100 mm × 350 mm in this study to evaluate the influence of steel fiber on concrete strength. The test setup diagram was shown in Fig. 2. Loads were arranged at a distance of 100 mm from supports. The displacement-controlled method was adopted and the loading rate was 0.5 mm/min. The vertical midspan deflection was measured by a linear variable differential transducer (LVDT).

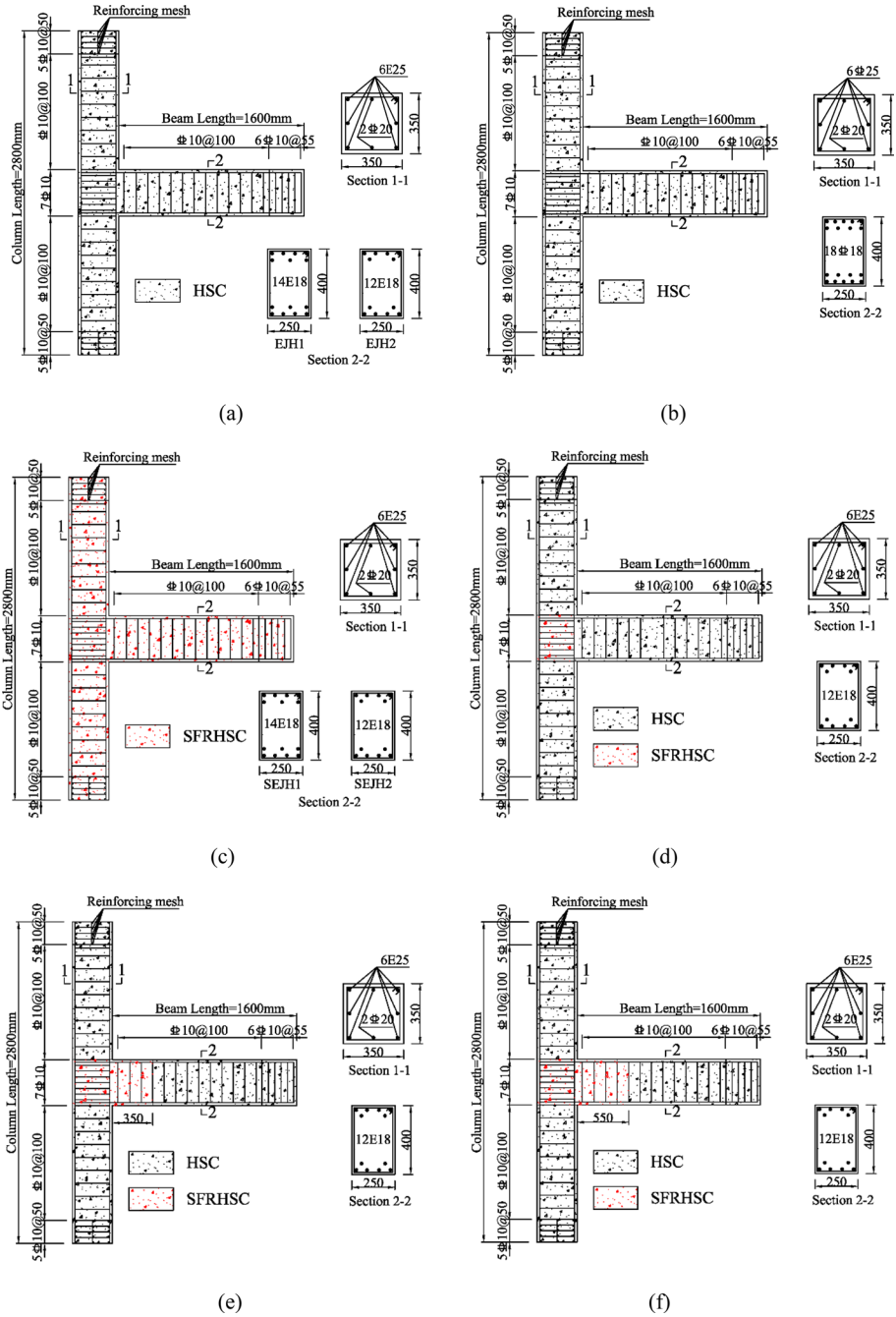


**Fig. 1** Detail of all specimens: **a** EJH1, EJH2, **b** EJN1, **c** SEJH1, SEJH2, **d** SEJH3, **e** SEJH4, and **f** SEJH5. Note: E represents grade 600 MPa steel bar, and ⌀ represents grade 400 MPa steel bar

**Table 3** Mechanical performance of concrete

| Concrete pattern | Cube compressive strength, $f_{cu}$ (MPa) | Tension strength, $f_t$ (MPa) | Elastic modulus, $E_c$ (GPa) |
|---|---|---|---|
| HSC | 55.6 | 2.96 | 35.4 |
| HSSFRC | 57.3 | 4.32 | 35.6 |

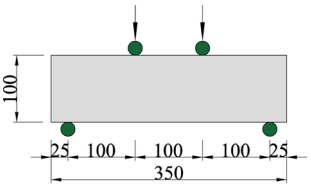


**Fig. 2** Test setup of four-point-bending tests

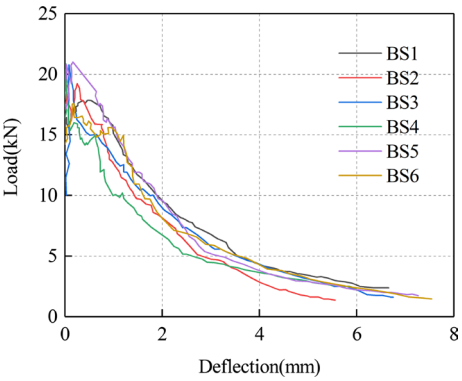


**Fig. 3** Load–deflection curves of HPFRCC specimens

Figure 3 shows the load–deflection curves of the four-point-bending specimens BS1-BS6. And the average flexural strength was 6.39 MPa.

Subsequently, the splitting tensile strength was calculated according to the empirical relation (1) obtained by Xu and Shi (2009),

$$f_{ft} = 1.63 f_{spt}^{0.89} \tag{1}$$

where $f_{spt}$ is the splitting tensile strength; $f_{ft}$ is flexural strength.

The tensile strength was 0.9 times splitting tensile strength. And the calculated tensile strength of HPFRCC was 4.18 MPa, which is also in good agreement with tension strength of 4.32 MPa obtained by our previous tension tests.

Furthermore, López et al. (2016) and Ríos et al. (2019) proposed a simplified inverse analysis method using four-point bending tests to determine the tensile properties of UHS-FRC, which also indicated the tensile strength can be calculated according to the flexural strength.

The reinforcements used in the test were HRB600 with the yield strength of 600 MPa and HRB400 with the yield strength of 400 MPa. Three different diameters and three different batches with lengths of 260 mm of bars were reserved to test the mechanical properties. According to GB/T 228-2010 (2010) uniaxial tensile test, the average measured the strength of the steel bars is shown in Table 4.

**Table 4** Mean measured strength of steel bars

| Material | Diameter (MPa) | Yield strength, $f_y$ (MPa) | Ultimate strength, $f_u$ (MPa) | Elastic modulus, $E_s$ (GPa) | Elongation (%) |
|---|---|---|---|---|---|
| HRB400 | 10 | 467 | 662 | 218 | 17.9 |
| HRB400 | 18 | 472 | 623 | 226 | 17.5 |
| HRB400 | 25 | 506 | 639 | 232 | 17.9 |
| HRB600 | 18 | 615 | 785 | 212 | 15.2 |
| HRB600 | 25 | 620 | 784 | 223 | 16.2 |

### 2.3 Test setup and loading pattern

The experimental test setup of exterior BCJs is shown in Fig. 4. The specimen was pinned via a hinge constraint at the bottom of the column and was roller supported at the top to simulate inflection points. The steel clip beams and the lateral bracings were used to connect to the reaction wall to prevent the column unexpected instability during the test. A vertical hydraulic jack was installed on the top of the column, and considered the column axial compression load for the beam-column joint in the prototype building, a vertical axial force of 505 kN (about 15% of the column's capacity) was applied to simulate the load transferred from the upper floors. A hydraulic jack with a capacity of 500 kN was fixed at the end of the beam to provide reversed cyclic loading. Two load transducers were installed on the hydraulic jacks on the column top and at the beam end. A linear variable differential transducer (LVDT) was installed at the end of the beam to measure the vertical displacement of the BCJs.

The loading history is shown in Fig. 5, which consisted of load-controlled patterns and displacement-controlled patterns in the test. The load-controlled patterns were adopted before the yielding of longitudinal reinforcements in the beams, and a load of each level was cycled once. And then, the load was switched to

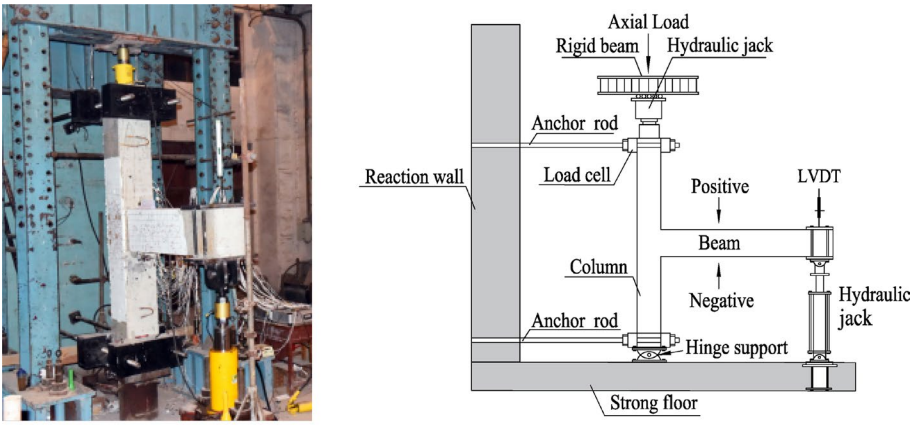


**Fig. 4** Test setup: **a** setup photograph and **b** schematic diagram of setup

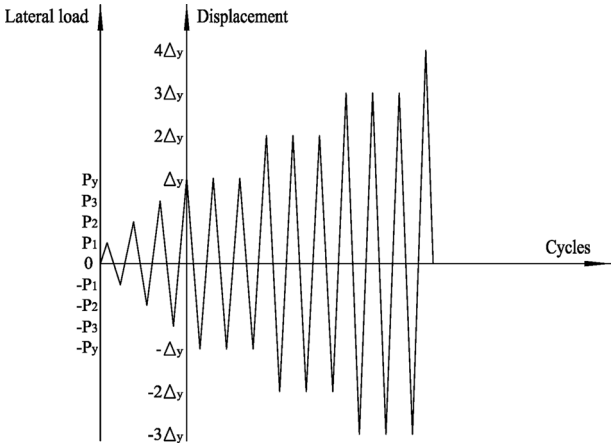


**Fig. 5** Loading history

displacement-controlled, and the displacement level gradually increased to $\Delta_y$, $2\Delta_y$, $3\Delta_y$, …, each displacement repeated three times until the load dropped to 85% of the peak load, and the specimen was failure.

All specimens were equipped with strain gauges and LVDTs to measure the strain values and deformation of the corresponding parts. Forty strain gauges with the spacing of 50 mm numbered 1–40 were attached at the upper and lower longitudinal reinforcements (see Fig. 6a). Two LVDTs 1–2 were installed in the core area of the joint and another two 3–4 were arranged at the beam ends to measure the shear deformation and rotation, respectively (see Fig. 6b). To measure the slip of the beam longitudinal bars, two dial indicators were arranged at the reserved short reinforcing bars. In order to make the short steel bar move freely along the longitudinal reinforcement of the beam, a plastic foam with dimensions of $30 \times 15 \times 25$ mm was placed on the short steel bar and the foam was pulled out before the test (see Fig. 6c).

## 3 Test results and discussion

### 3.1 Crack patterns and failure modes

Figure 7 shows the crack patterns and failure modes of eight exterior BCJs. The crack patterns of specimens were very similar. The vertical bending cracks first appeared in the tensile zone at the end of the beam and then gradually extended. Then the diagonal crack occurred in the joint core area, which was under diagonal tensile and compression stresses owing to the principle tensile stress over the tensile strength of HSC or HSSFRC. The occurrence of shear cracks caused the premature slipping of HSS reinforcements and HSC crushing at the beam-column interface and joint core resulting in shear failure.

The protective layer concrete in the core of the joint EJN1 almost all fell off. For joints EJH1 and EJH2, few concrete spalling formed in the beam-column interface due to the bond-slip cracks because it adopted HSS reinforcements in the beam. The concrete crushing of joint EJH1 was a little more severe than the specimen EJH2 in the joint due to the former having a higher shear compression ratio, which had a much adverse effect on the failure mode of the joints. Specimens EJH1 and EJH2 had 22% and 33% less beam

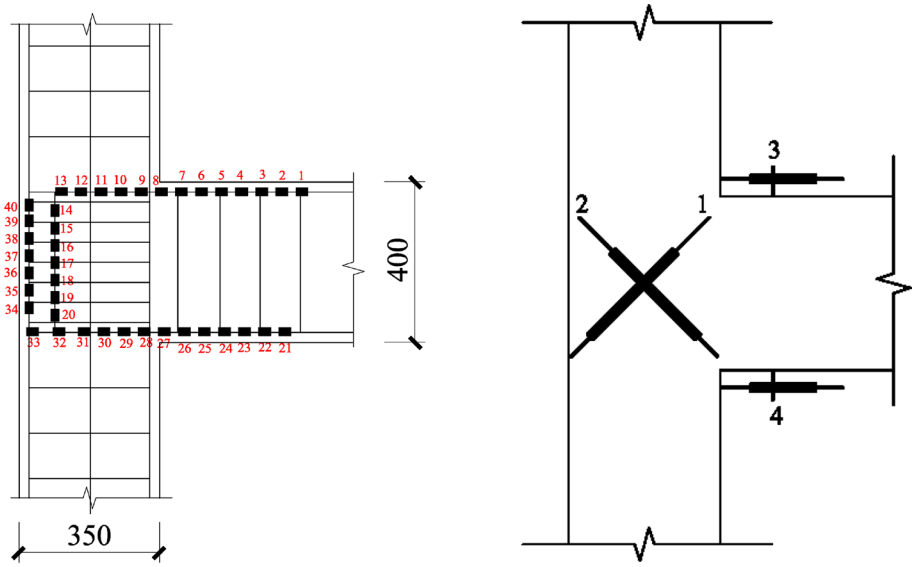


(a) (b)

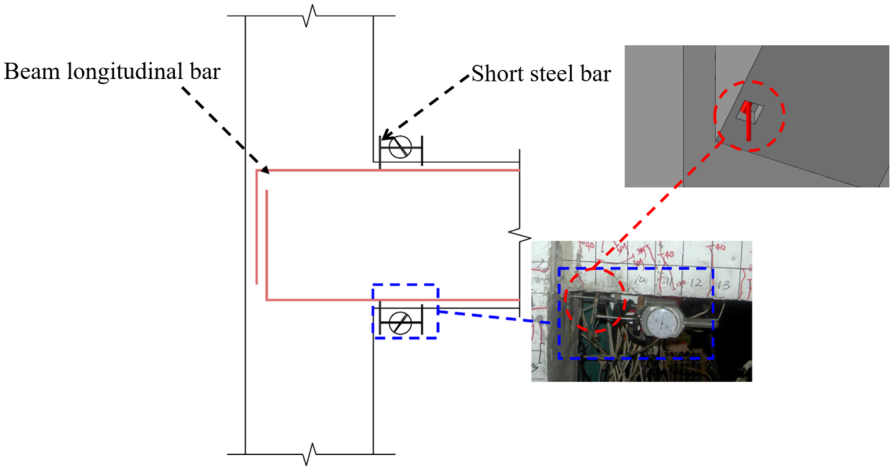


(c)

**Fig. 6** Layout of strain gauges, LVDTs and dial indicators: **a** layout of strain gauges at longitudinal reinforcements of the beam, **b** layout of LVDTs, and **c** layout of dial indicators

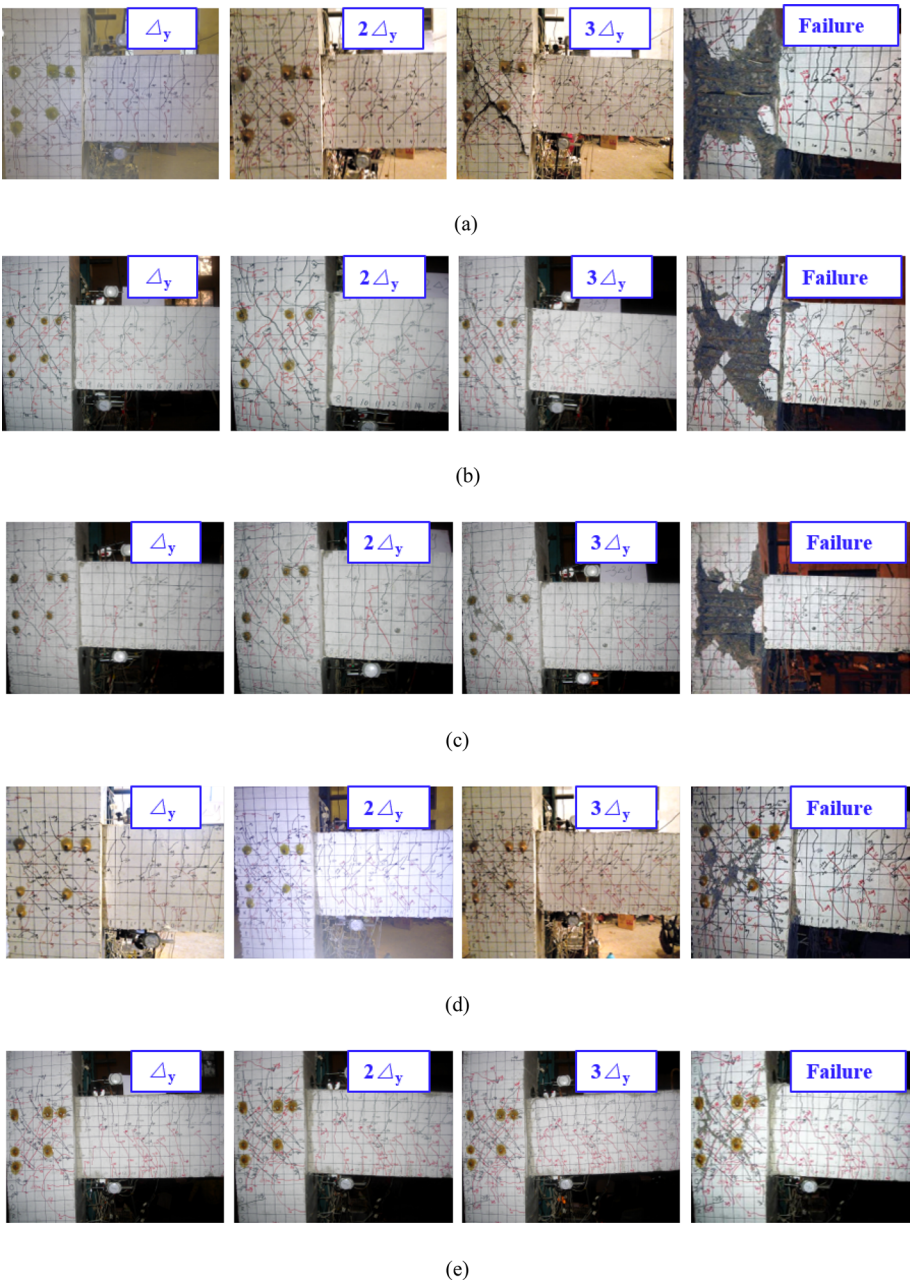


**Fig. 7** Crack patterns and failure modes of all specimens: **a** EJH1, **b** EJH2, **c** EJN1, **d** SEJH1, **e** SEJH2, **f** SEJH3, **g** SEJH4, and **h** SEJH5

reinforcements, respectively, compared to EJN1, and occurred in shear failure and bond failure of the beam longitudinal reinforcement. Therefore, the bond strength between HSS reinforcements and HSC should be improved and the anchoring length should be enhanced.

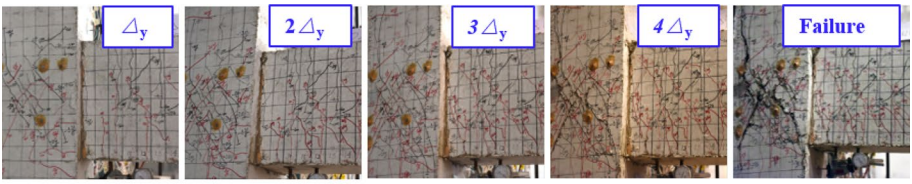


(f)

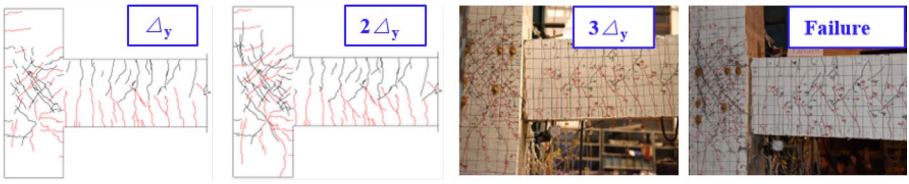


(g)

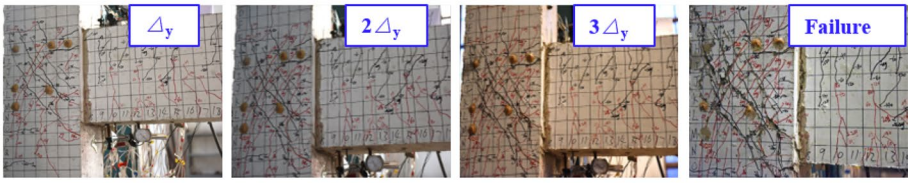


(h)

**Fig. 7** (continued)

Compared with those beam-column joints with HSC and normal-strength steel bars, the HSS reinforcements in HSSFRC initially yielded at higher load and displacement due to better consistency between HSS reinforcements and HSSFRC, larger cohesion and bonding strength, and higher deformation tolerance before failure in HSSFRC. From the Fig. 7 and Table 5, using HSSFRC could significantly enhance the crack load and load bearing capacity compared with specimens with HSC. This phenomenon was attributed to steel fiber delaying the initiation of internal micro cracks, forcing cracks further development to absorb more energy, thus the load bearing capacity was enhanced. The usage of HSSFRC materials enhanced the tensile strength and alleviated shear failure by improving bond strength due to the steel fiber bridging effect, which could delay the slippage of HSS reinforcements in the beams. There was no concrete crushing in beam-column joints with HSSFRC accompanied by opening or closing of cracks. Finally, the specimens with HSSFRC and HSS reinforcement occurred joint shear failure accompanied by the yielding of the beam longitudinal HSS reinforcements.

Specimens SEJH3-SEJH5 with HSSFRC in different concreting patterns exhibited similar cracking development and failure modes compared to SEJH2 with HSSFRC in the entire specimen. For specimen SEJH4 with an HSSFRC area of 350 mm, the fine and dense cracks concentrated in the steel fiber reinforced region after yield load, and the width increased along with hairline cracks. While specimen SEJH5 with an HSSFRC area of 550 mm, the cracks spreading region was much larger and the number in the steel

**Table 5** Test results

| Spec | $P_{cr}$ (kN) | $P_y$ (kN) | $P_u$ (kN) | $\Delta_y$ (mm) | $\Delta_u$ (mm) | $\mu$ | $E_t$ (kN m) | $K_{i0}$ (kN/mm) | $K_r$ (%) |
|---|---|---|---|---|---|---|---|---|---|
| EJH1(+) | 92.5 | 170.8 | 246.2 | 21.5 | 85.1 | 3.97 | 42.4 | 19.4 | 16.9 |
| EJH1(−) | 63.3 | 189.1 | 238.1 | 27.9 | 85.2 | 3.05 | | | |
| EJH2(+) | 84.0 | 144.2 | 212.3 | 22.3 | 90.9 | 4.08 | 42.6 | 21.9 | 15.1 |
| EJH2(−) | 79.9 | 167.2 | 204.9 | 29.1 | 95.3 | 3.27 | | | |
| EJN1(+) | 90.1 | 156.3 | 217.1 | 15.0 | 59.2 | 3.96 | 33.3 | 15.1 | 17.3 |
| EJN1(−) | 84.0 | 187.5 | 225.9 | 33.3 | 89.6 | 2.69 | | | |
| SEJH1(+) | 87.7 | 176.6 | 243.1 | 22.9 | 90.4 | 3.95 | 45.3 | 12.2 | 19.2 |
| SEJH1(−) | 62.3 | 171.2 | 237.7 | 24.7 | 90.3 | 3.66 | | | |
| SEJH2(+) | 80.9 | 165.6 | 220.5 | 22.9 | 100.7 | 4.39 | 51.0 | 14.9 | 14.9 |
| SEJH2(−) | 91.4 | 190.9 | 229.9 | 29.9 | 106.2 | 3.55 | | | |
| SEJH3(+) | 82.9 | 143.6 | 207.6 | 19.6 | 94.0 | 4.79 | 41.0 | 10.7 | 17.9 |
| SEJH3(−) | 83.6 | 166.8 | 208.5 | 27.2 | 97.9 | 3.6 | | | |
| SEJH4(+) | 85.3 | 144.2 | 198.9 | 22.0 | 102.1 | 4.65 | 36.3 | 12.7 | 18.0 |
| SEJH4(−) | 82.3 | 164.7 | 218.6 | 26.7 | 90.3 | 3.38 | | | |
| SEJH5(+) | 79.9 | 168.5 | 228.9 | 22.9 | 99.7 | 4.35 | 38.1 | 12.5 | 18.3 |
| SEJH5(−) | 82.0 | 170.4 | 199.5 | 29.1 | 91.4 | 3.14 | | | |

Spec., Specimens; (+), positive load; (−), negative load; $P_{cr}$, crack load; $P_y$, yield load; $P_u$, peak load; $\Delta_y$, yield displacement; $\Delta_u$, maximum displacement; $\mu$, ductility ($\Delta_u/\Delta_y$); $E_t$, total cumulative energy dissipation; $K_{i0}$, initial stiffness; $K_r$, retained stiffness ratio in the failure stage

fiber reinforced region was more than those without HSSFRC. On the contrary, specimen SEJH2 with HSSFRC area of the whole beams, much more fine and dense cracks spread to the support. There was no concrete crushing in these beam-column interfaces and joints with HSSFRC of a certain length in beams accompanied by opening or closing of cracks. But SEJH3 with HSSFRC only in the joint, the concrete spalling at the beam-column interface after slippage of HSS reinforcement at the beam end, followed by severe shear cracks formation and concrete spalling in the joint. Based on the crack observation and concrete spalling, HSSFRC area could induce a certain length of crack development and HSSFRC area of 1.5 times of effective beam height (550 mm) in the beams was efficient for reinforcing the area to achieve better bonding performance of HSS reinforcements and HSSFRC.

### 3.2 Hysteretic behavior

The hysteretic curves of all specimens are shown in Fig. 8, reflects the relationship between the load and displacement of eight specimens under quasi-static cyclic loading. The shape of the hysteretic hoop of the BCJs gradually developed from shuttle shape to bow shape. In the initial loading stage, the load and displacement increased linearly showed the specimens were in elastic stage. With the development of cracks and the number of cycles, the deformation of specimens increased nonlinearly due to plastic deformation. Finally, the slope of hysteresis curve decreased as well as the strength of the joints degraded continuously. The pinching performance in the curves was related to the reinforcement slippage, tensile cracks, concrete spalling and shear failure.

Compared with specimen EJN1, the hysteretic curves of EJH1 and EJH2 with the reduction of 22.6% and 33.3% longitudinal reinforcement ratio, respectively, were

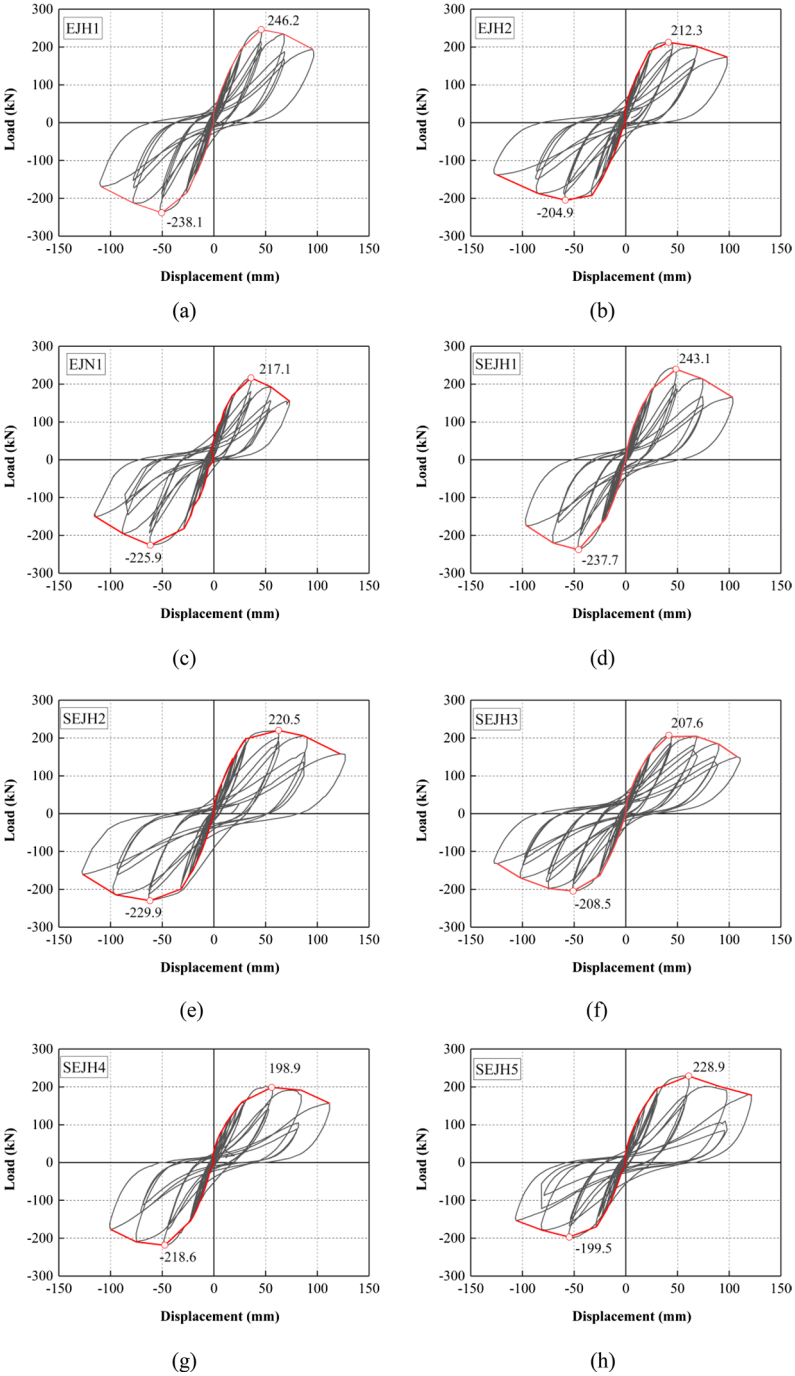


**Fig. 8** Hysteretic relationships of all specimens: **a** EJH1, **b** EJH2, **c** EJN1, **d** SEJH1, **e** SEJH2, **f** SEJH3, **g** SEJH4, and **h** SEJH5

wider, and the peak load and maximum displacement were larger. This indicated that the efficacy of HSS bars in hysteretic area, load bearing capacity and deformation capacity of BCJs. Furthermore, EJH2 specimen showed a narrower hysteretic hoop and severer pinching than EJH1 due to the latter having the higher shear compression ratio, which derived from bond-slip of beam longitudinal reinforcements. Therefore, sufficient anchorage length was important in the hysteretic performance of exterior BCJs reinforced by HSS bars. Alavi-Dehkordi et al (2019) also reported the same results.

The usage of HSSFRC and HSS reinforcement materials in beam-column joints improved capacity and deformation capacity and enhanced the loop area without apparent strength and stiffness degradation compared to specimen EJN1, which was attributed to the effect of steel fiber bridging, enhancing the bonding strength of HSSFRC and HSS reinforcements. The hysteresis curves of specimens SEJH1 and SEJH2 reinforced by HSSFRC were wider than those of specimens EJH1 and EJH2 with HSC, and the pinching in the middle of the hysteresis loop was improved. Compared with EJH2, the post-yield behavior and final deformation of specimens SEJH3-SEJH5 were improved. This can be attributed to the improved tensile strength, the good bonding capacity of HSSFRC and HSS reinforcements resulting in smaller slippage of HSS bars. While the specimens SEJH3-SEJH5 reinforced by HSSFRC in different regions exhibited similar hysteresis response when compared with HSSFRC used in entire specimen, which was because HSSFRC delayed the occurrence and propagation of the shear cracks, especially in the joint region. Moreover, the specimens SEJH4 and SEJH5 reinforced with HSSFRC in the joint area and 1–1.5 times of effective beam height had better hysteretic performance than the specimen SEJH3 with HSSFRC only in the joint. In general, the hysteretic curves were stable due to slight damage in the joint and small slippage of longitudinal HSS reinforcements, and the joints exhibited stable performance up to the displacement of 90 mm, which indicated that the joints with HSS reinforcements and HSSFRC was suitably designed to withstand the seismic load.

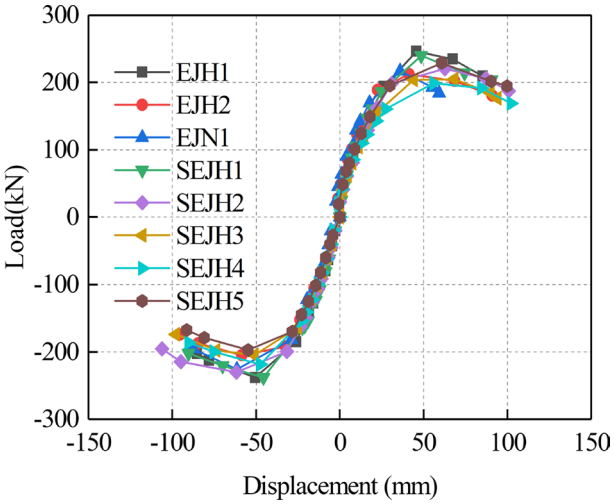


**Fig. 9** Envelop curves of beam-column joint specimens

### 3.3 Envelope curves and ductility

Figure 9 shows the load–displacement skeleton curves of exterior BCJs, which responded to the deformation capability and bearing capacity of joints. Specimens with HSS bars experienced a longer yield stage than EJN1 indicated better deformation capacity. At the later stage, the deformation capacity of specimens EJH1 and EJH2 were larger than that of specimens EJN1 for the former using HSS bars, which improved the ductility of the joints (see Table 5). The specimen EJH1 with higher shear compression ratio represented better bearing capacity compared with specimen EJH2 under the same displacement level. The bearing capacity of SEJH1 and SEJH2 were nearly similar to EJH1 and EJH2, which concluded that steel fiber had little effect on the improvement of load capacity. The load degradation rate of specimens EJH1 and EJH2 was faster than that of specimens SEJH1-SEJH5 due to the former having more severe concrete spalling. It is because the better bonding performance of HSS reinforcements and HSSFRC prevented the early slippage of beam reinforcement and reduced the load degradation rate during cyclic loading. Although the compressive strength of HSC and HSSFRC was comparable, the maximum deformation of all specimens SEJH1-SEJH5 with steel fiber reinforced concrete was greater than that with HSC due to HSSFRC having higher tensile strength and improved HSSFRC bonding with HSS reinforcements. These results were attributed to the bridging effect of steel fibers and the mechanism of anti-cracking, which allowed larger deformation under the same condition. In general, HSSFRC improved the post-yield behavior of specimens, but it is basically the same in the elastic range.

Ductility, $\mu$, one of the important indicators of seismic performance, is defined as the ratio of maximum displacement ($\Delta_u$) corresponded to 85% of the peak load to yield displacement ($\Delta_y$). Yield displacement is usually assessed based on two different methods: balance of energy and general yielding (Dabiri et al. 2020; Li et al. 2013; Kheyroddin et al. 2021). The method used in this study is based on the balance of energy as shown in Fig. 10. A secant line passing the origin point O and a point I on the curve intersected the peak load at point A. The secant line should be moved to obtain two equal shaded areas. Thus, point A is regarded as the yield displacement.

The ductility of specimen EJN1 was least due to serious concrete crushing and spalling in the joint core area. While the ductility of specimens EJH1 and EJH2 were improved by using HSS bars resulting in larger maximum displacement. The ductility of specimen EJH2

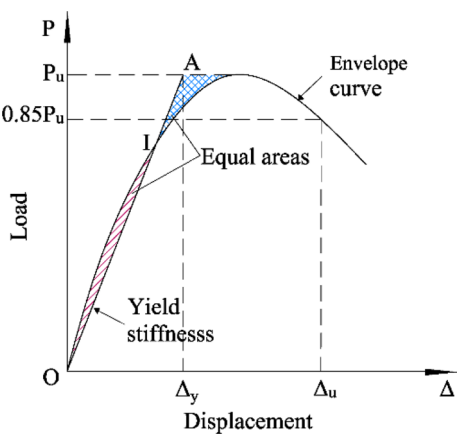


**Fig. 10** Definitions of yield and maximum displacement

was greater than that of specimen EJH1, because the reduction of shear compression ratio improved the deformation capacity. Specimens SEJH1 and SEJH2 exhibited 14% and 17% greater ductility than specimen EJN1, which due to the better bonding of HSS bars and HSSFRC resulted in the increased deformability and ductility of these specimens. When the HSSFRC was used in the joint core and extended to the beam end at a distance also enhanced the ductility obviously, which was consistent with the slower drop of the skeleton curve. The decreased of ductility in specimens without HSSFRC was mainly related to the slippage of longitudinal HSS bars and the concrete spalling in the plastic hinge and joint region. And with the increase of the application range of HSSFRC, the improvement effect gradually decreased for specimens SEJH3-SEJH5.

### 3.4 Stiffness degradation

Stiffness degradation is also one of the important indexes of seismic performance of the structures, which reflects the degradation process of structural stiffness. Stiffness degradation is assessed by the secant stiffness variations in each cycle. The secant stiffness, $K_i$, is calculated as:

$$K_i = \frac{|+F_i| + |-F_i|}{|+\Delta_i| + |-\Delta_i|} \tag{2}$$

where $+F_i$ and $F_i$ represent the maximum load in the positive and negative direction of the $i$th cycle, respectively; $+\Delta_i$ and $-\Delta_i$ represent the equivalent displacement of the $i$th cycle, respectively.

Figure 11 shows the stiffness degradation curves. It is worth mentioning that the stiffness decreased with the increase of the displacement, which was determined by the increase of accumulated damage in the specimens. The secant stiffness degraded faster before yielding due to the occurrence and development of cracks, and then the displacement increased faster while the load increased slower, and the slope of the stiffness degradation curve decreased gradually. When reaching the peak load, the displacement increased

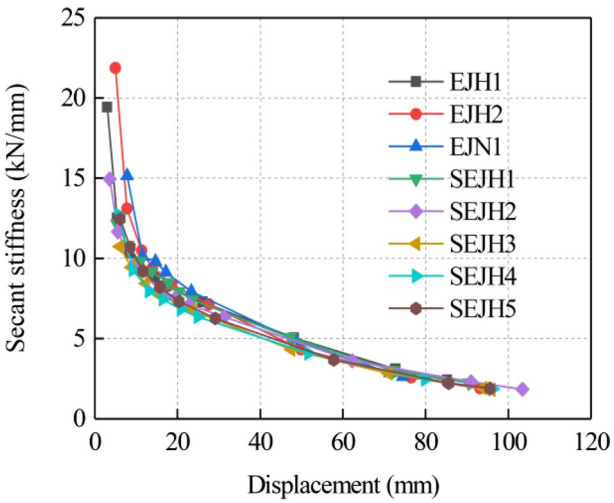


**Fig. 11** Stiffness degradation curves

rapidly as the load changed little, and the stiffness degradation curve was gentle. Specimens with HSS bars exhibited similar secant stiffness to that made of normal-strength steel bars. This showed the efficiency of the beam and column longitudinal reinforcements with HSS bars in specimens EJH1 and EJH2 while the beam-column longitudinal reinforcements were reduced by over 22%. The spreading steel fibers had the advantage of controlling crack propagation. This behavior could result in higher energy requirements for steel fiber debonding and pulling out near the cracks. Thus, the stiffness degradation of the specimens SEJH1-SEJH5 with HSSFRC was much slower.

The stiffness degradation ratio, normalized to a dimensionless parameter to eliminate the influence of the initial stiffness and obtained by dividing each secant stiffness value of the specimens by the initial secant stiffness, versus displacement curves are shown in Fig. 12. The stiffness degradation ratio of the two specimens EJH1 and EJH2 with HSS were higher than EJN1, due to the large number of flexural and shear cracks as well as accompanied by severe concrete spalling that occurred in EJN1. Specimens EJH1 and EJH2 had a lower stiffness degradation ratio than the five specimens with HSSFRC, which can be attributed to strain hardening by improving the tensile deformability of concrete through reinforced with steel fiber in the joint and plastic hinge area and insufficient bonding between the beam longitudinal reinforcement with HSS bars and HSC due to inadequate development length. While HSS bars coupled with HSSFRC could alleviate the stiffness degradation rate. In general, the stiffness degradation of specimens SEJH1-SEJH5 with HSSFRC was much slower due to the improved cracking resistance and tensile strain after yielding. Specimen SEJH5, which was reinforced with steel fiber in the joint and 1.5 times of effective beam height, had the slowest stiffness degradation. Furthermore, the remained stiffness of specimens SEJH3-SEJH5 was also relatively higher (see Table 5), indicating that HSSFRC had the ability to maintain enough strength and stiffness after failure.

### 3.5 Energy dissipation and damping ratio

The energy dissipation capacity of BCJs is an important parameter to evaluate seismic performance, which is equal to the enclosed area of a hysteresis loop. And the cumulative energy dissipation is calculated by summing the areas of all hysteretic loops.

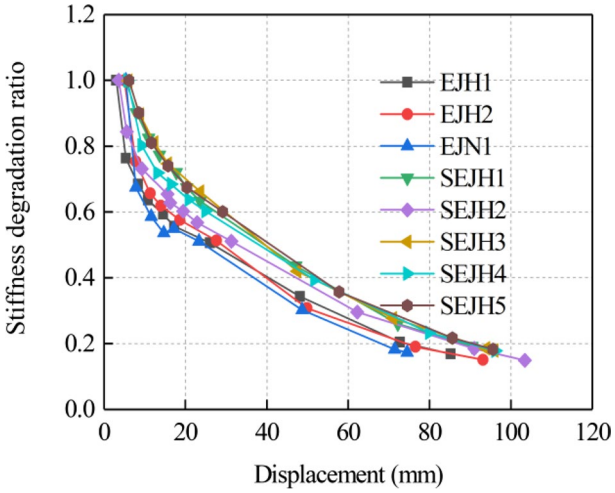


**Fig. 12** Stiffness degradation ratio versus displacement curves

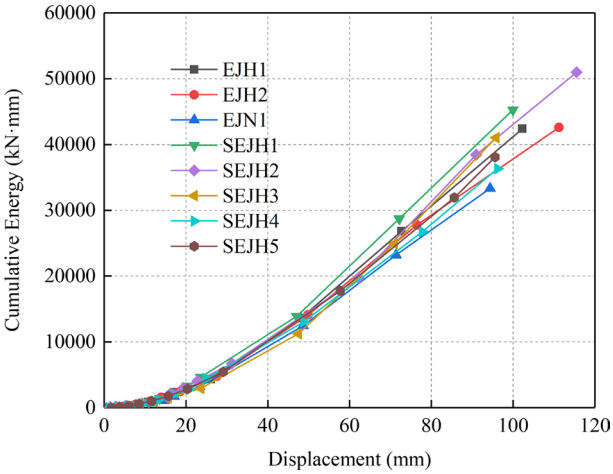


**Fig. 13** Cumulative energy dissipation curves

Figure 13 shows the cumulative energy dissipation of all exterior joint specimens against the displacement. At the initial stage, the cumulative energy dissipation of each joint was similar, and the difference increased when the displacement exceeded 30 mm. Compared with specimen EJN1, the cumulative energy dissipation of specimens EJH1 and EJH2 increased about 28%, showed that the efficiency of HSS bars when used as the beam longitudinal reinforcements with a reduced amount of over 22% for larger hysteretic loops and higher bearing capacity. Moreover, a larger bond-slip of beam reinforcements occurred in specimen EJN1 resulting in lower energy dissipation.

SEJH1 and SEJH2 had the largest cumulative energy dissipation, which were 6% and 20% higher than EJH1 and EJH2 (see Table 5), respectively, indicating that HSSFRC had significant advantages in improving the energy consumption capacity of BCJs. This was mainly due to steel fiber in HSC restrained the development of cracks and improved the concrete spalling. Moreover, SEJH1 and SEJH2 had wider hysteretic hoops and higher load capacity made with HSS bars coupled with HSSFRC, indicating that the efficiency of HSS bars in energy dissipation because of excellent bond strength between HSS bars and HSSFRC. While the HSSFRC in different concreting regions has little significant positive effect on energy dissipation. Additionally, the specimens SEJH3 with the smallest HSSFRC placement region among specimens SEJH1-SEJH3 showed the highest cumulative energy dissipation due to the relatively severe damage in the joint area.

The increasement in the cumulative energy dissipation was mainly due to higher tensile strength of HSSFRC and HSS reinforcement material. The higher tensile strength of HSSFRC was mainly dependent on the steel fiber energy absorption mechanism, which governed the improvement of the joint performance. The limited enhanced compressive strength could not alleviate joint shear failure. These findings were in agreement with the experimental results performed by Saghafi and Shariatmadar (2018).

Generally, the equivalent viscous damping ratio is used to measuring the energy dissipation capacity of structures, and the equivalent viscous damping ratio, $h_e$, is calculated according to formula (3) (Wang et al. 2017).

$$h_e = \frac{1}{2\pi}\frac{S_{ABCD}}{S_{OCF} + S_{OAE}} \tag{3}$$

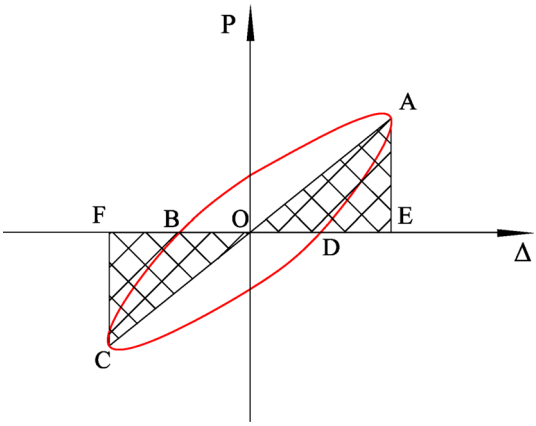


**Fig. 14** Definitions of equivalent viscous damping ratio

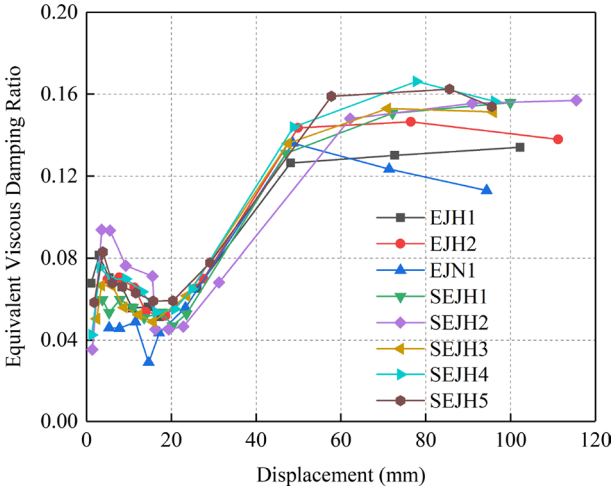


**Fig. 15** Equivalent viscous damping ratio-displacement curves

where the area of hysteresis loop $S_{ABCD}$ represents the energy dissipated by the member under the loading cycle, and the sum of area $S_{OCF}$ and $S_{OAE}$ show the energy absorbed (see Fig. 14). It can be seen from Fig. 15 that the equivalent viscous damping ratio of the specimen was small with a downward trend before yielding and increased rapidly after yielding. When reaching the peak load, the equivalent viscous damping ratio began to decrease slowly.

The specimens EJH1 and EJH2 showed higher equivalent viscous damping ratio than EJN1 before yielding, and the growth rate were faster after yielding, but the decline rate was slower than EJN1. These results showed that HSS bars improved the elastic deformation and inelastic deformation of the exterior BCJs under cyclic loading, thus enhanced energy dissipation capacity. The equivalent viscous damping ratio of specimen EJH1 was smaller than EJH2, as the shear compression ratio increased resulting in the energy dissipation capacity decreased. Due to the proper bonding between HSS and HSSFRC, the absence of pinching and larger hysteresis loop, the HSSFRC specimens have higher equivalent hysteresis damping coefficient than the HSC specimens. These results showed that HSSFRC was conducive to the energy dissipation capacity

as the steel fiber in the HSC transferred the stresses across the joints in some extend. Compared with the fiber reinforced specimens, the equivalent viscous damping ratio of specimens SEJH4 and SEJH5 was the highest, and the energy dissipation capacity was the strongest at the later stage of loading.

### 3.6 Joint shear deformation

In this test, two LVDTs showed in Fig. 6b were placed in the diagonal direction of the core area, respectively, which were used to measure the expansion and contraction of cores, then the shear deformation of the joint can be calculated through the geometric relationship. The shear deformation, $\gamma$, in the joint is shown in Fig. 16 and is calculated by Eq. (4) as follows:

$$\gamma = \frac{\sqrt{b^2 + h^2}}{2bh}\left(\left|\delta_1 + \delta_1'\right| + \left|\delta_2 + \delta_2'\right|\right) \tag{4}$$

where $b$ and $h$ are the width and height of the joint cores between the LVDTs, respectively, $\delta_1 + \delta_1'$ and $\delta_2 + \delta_2'$ are the deformations of two LVDTs, respectively.

According to Eq. (4), the shear deformation in the core area of each exterior joint was calculated. Figure 17 shows the shear force versus shear deformation hysteretic curves of each exterior joint.

There was a small shear deformation before specimens yielded. After that, the shear deformation increased obviously, which attribute to concrete spalling and diagonal cracks development. The use of HSS reinforcements in specimens increased the shear deformation and shear force of joints. In addition, the shear deformation of joints was significantly reduced with the smaller shear compression ratio. This trend was more significant in HSS reinforcement specimens. Unlike the specimens EJH1 and EJH2, the shear deformation of joints SEJH1-SEJH5 with HSSFRC decreased. And the maximum shear deformation of the specimens SEJH3-SEJH5 reinforced with HSSFRC in different regions was smaller than the unreinforced specimen EJH1. As HSSFRC with higher tensile strength limited the development of cracks and reduced the shear deformation of the joint core.

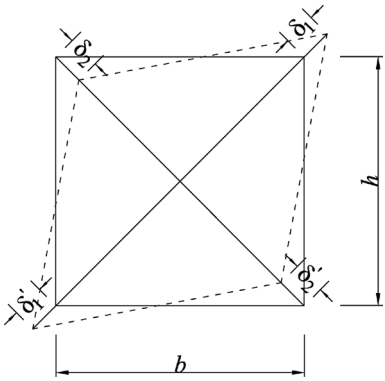


**Fig. 16** Shear deformation of joint core area

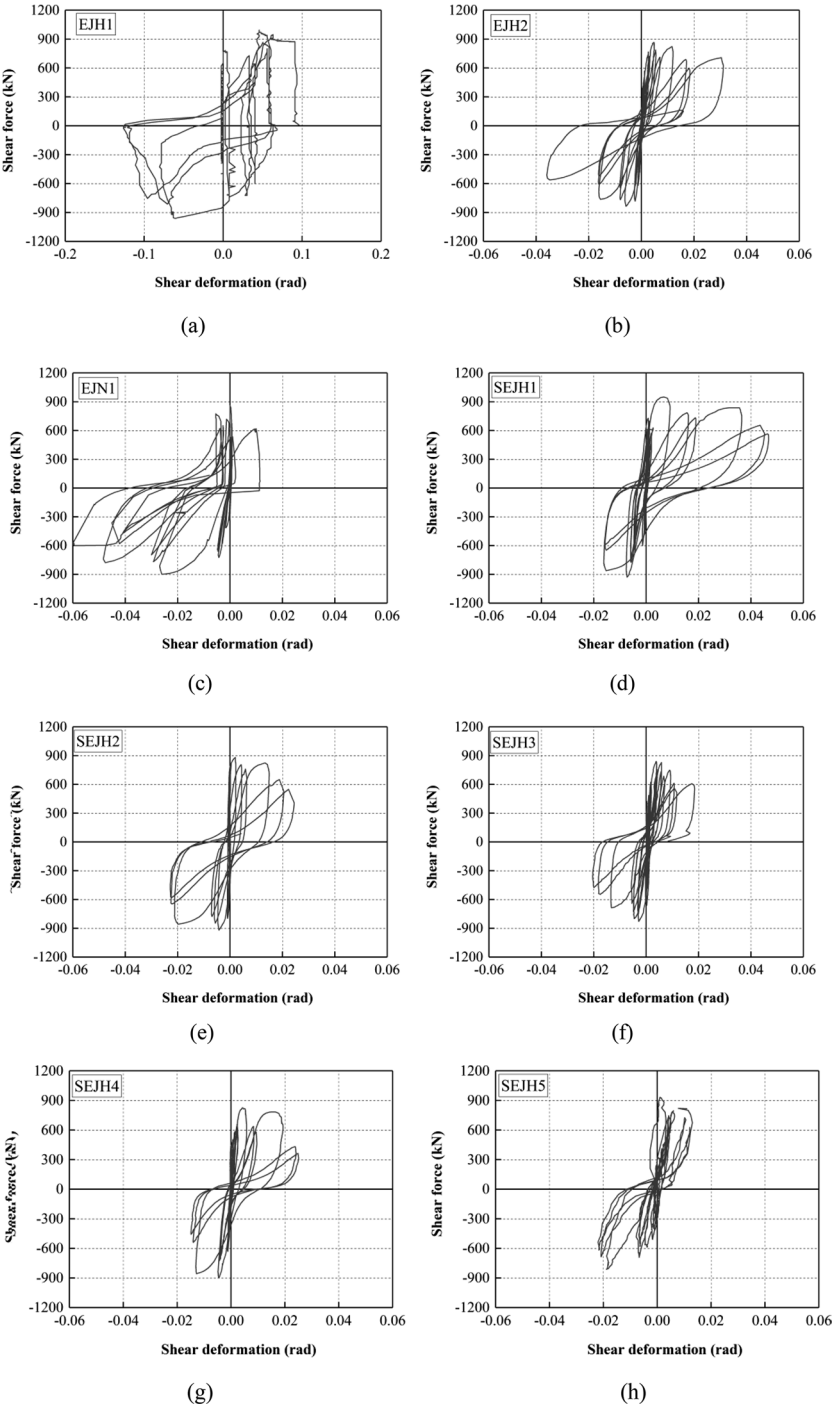


**Fig. 17** Hysteretic curves of shear force-shear deformation: **a** EJH1, **b** EJH2, **c** EJN1, **d** SEJH1, **e** SEJH2, **f** SEJH3, **g** SEJH4, and **h** SEJH5

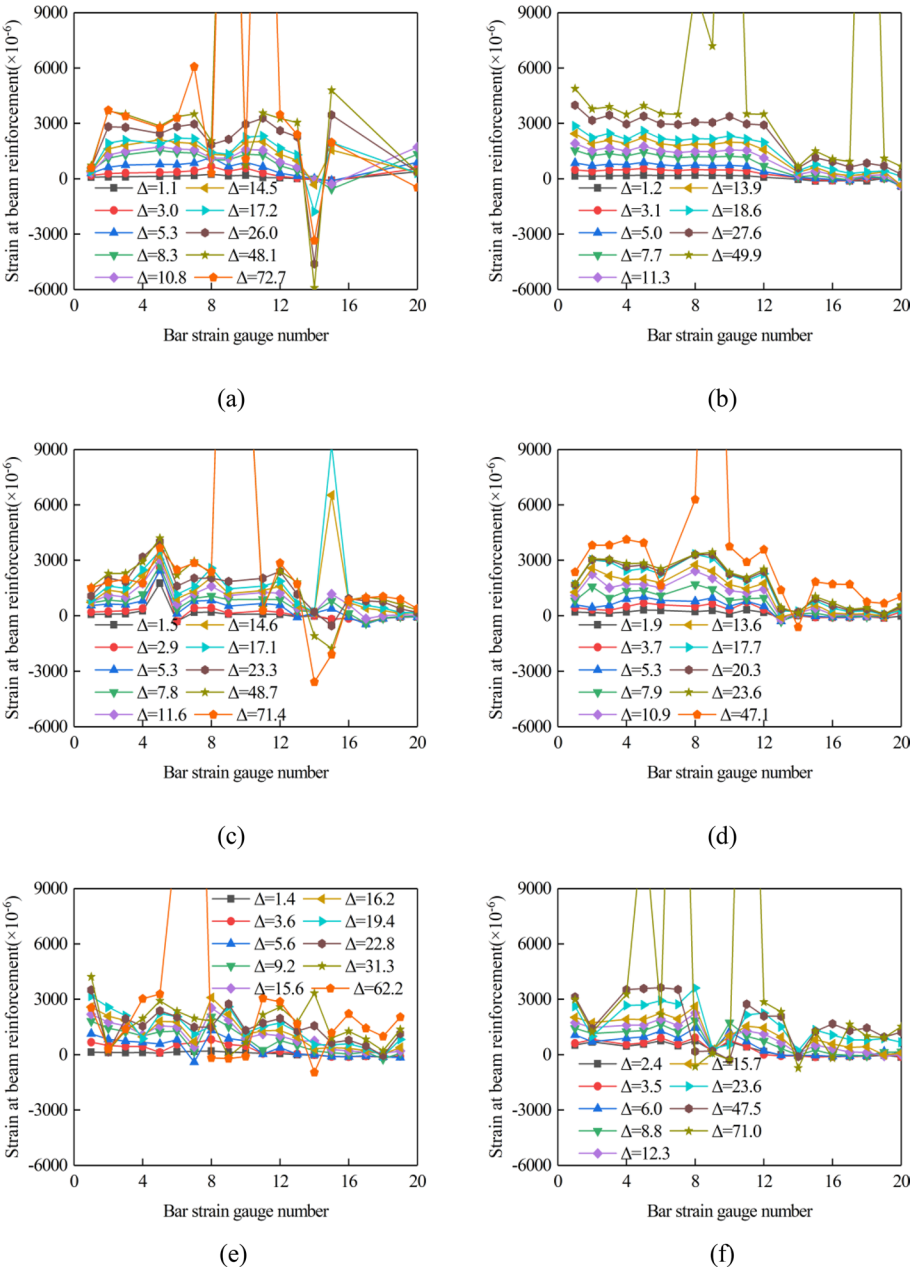


**Fig. 18** Strain curves of longitudinal reinforcements of beams: **a** EJH1, **b** EJH2, **c** EJN1, **d** SEJH1, **e** SEJH2, **f** SEJH3, **g** SEJH4, and **h** SEJH5

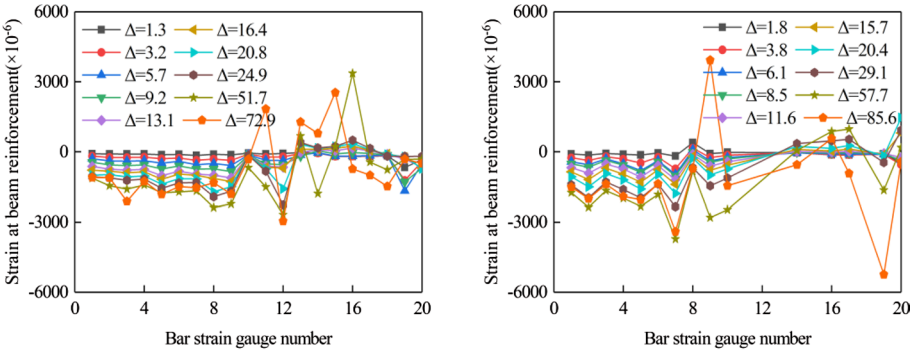


(g) (h)

**Fig. 18** (continued)

### 3.7 Strains of the beam longitudinal reinforcements

The measured strains of the upper and lower beam longitudinal reinforcements of the first cycle under different displacement loading is shown in Fig. 18. With the appearance and expansion of diagonal cracks in the core area, the longitudinal reinforcements at the hook of the beam reinforcements yielded, where the strain had exceeded the yield strain when the reinforcements at the end of the beam yielded, and tensile strain at the low part was larger and more uniform.

The tensile strains of the horizontal section at the anchorage end and the beam end were higher, and the yielding of the reinforcements permeated from the beam end to the anchorage end, which led to the bond degradation of the beam reinforcements under reversed cyclic loading. With the increasing displacement, the strain at the vertical section enhanced slightly, and the strains were almost zero at the end of the vertical section. Compared with specimen EJN1, the strains of beam reinforcements in specimen EJH1 were similar to specimen EJH2. The tensile strain at the beam end and horizontal anchorage section increased, and the maximum tensile strain occurred at the beam end and the hook of beam reinforcements. The strains of the specimen EJH2 with lower shear compression ratio were more uniform, while the strains of the vertical section increased slightly. Unlike the specimens EJH1 and EJH2, the tensile strains of the beams in the specimens SEJH1 and SEJH2 were more uniform, and the tensile strains at the end and horizontal anchorage section were reduced, because the crack distribution and development in the core area were more uniform with the addition of HSSFRC. And HSSFRC limited the occurrence and development of cracks and enhanced the bonding of beam reinforcements. Also, the specimens SEJH4 and SEJH5 exhibited more uniform strains than specimen SEJH3, and the tensile strains of the beam reinforcements at the beam end and the horizontal anchorage section were greatly reduced, indicating that HSSFRC limited the occurrence and development of cracks and enhanced the bonding of beam reinforcements.

### 3.8 Degradation of the bond stress

The oblique cracks in the joint core area were extended after beam longitudinal bars were yielded. Under the cyclic loading, the slip of beam longitudinal reinforcements caused an adverse effect on the measurement of the beam reinforcement strain. However, it can be considered that the strains of the beam bars through the joint segment are linear from the general trend of the test results. Thus, the bond stress between the beam bars through the joint segment and the concrete was distributed evenly. Therefore, by measuring the strain values of the beam longitudinal bars at the beam-column interface, the average bonding stress $\tau_b$ on the surface of the beam longitudinal bars across the joint section under different loading can be calculated according to Eq. (5) (Harajli et al. 2002).

$$\tau_b = \frac{T_{br} - C_{sl}}{h_c S_b} \tag{5}$$

where $T_{br}$ and $C_{sl}$ are the tension and compressive force of the upper bars at the beam-column interface, respectively. The tension force was regarded as positive and the compressive force was defined as negative. $h_c$ is the length of the horizontal anchoring segment; $S_b$ is the perimeter of reinforcements.

The bond stress ratio is the ratio of average bond stress $\tau_b$ to the ultimate average bond stress $\tau_{bu}$, and bond stress ratio versus displacement ratio relationship of all specimens is shown in Fig. 19. The bond stress ratio of specimen EJH1 decreased faster compared with EJH2, which indicated that reduced the shear compression ratio could slow down the bond degradation of beam reinforcements in both loading directions. The bond stress ratios of specimen EJN1 was much lower than the other specimens with HSS bars, regardless of HSSFRC, which showed that the bond degradation performance of high-strength reinforcements was enhanced. The bond degradation of the specimens SEJH1-SEJH5 with HSSFRC was better than specimens with HSC, showing the excellent bond performance of the combination of HSSFRC and HSS bars.

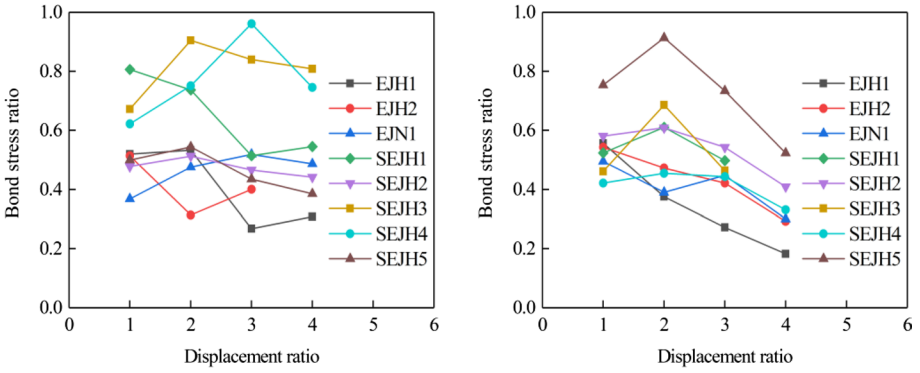


**Fig. 19** Bond stress curve: **a** positive, and **b** negative

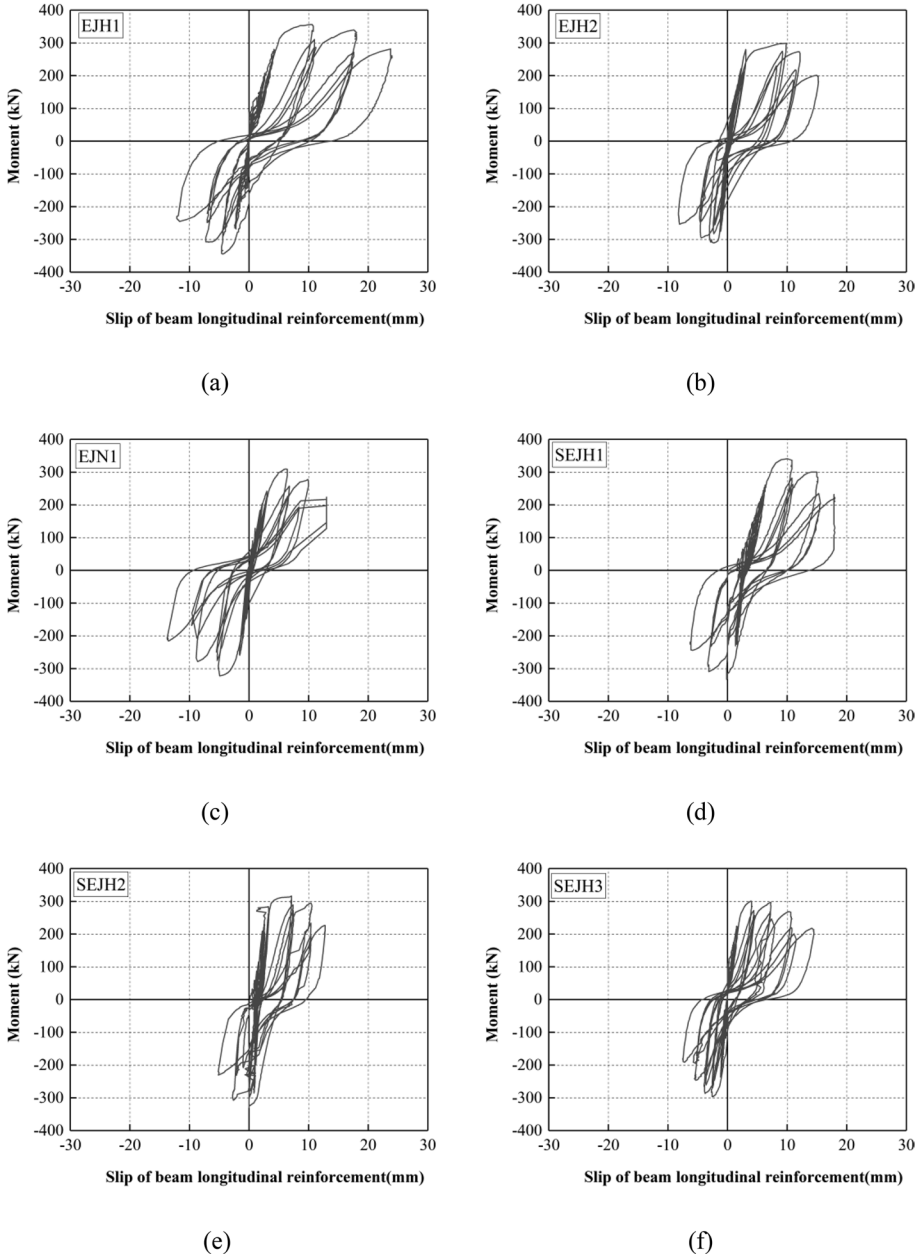


**Fig. 20** Moment-Slip of beam longitudinal reinforcement curves: **a** EJH1, **b** EJH2, **c** EJN1, **d** SEJH1, **e** SEJH2, **f** SEJH3, **g** SEJH4, and **h** SEJH5

### 3.9 Slippage of the beam longitudinal reinforcements

The hysteretic curves of the moment of beam end and slip of beam longitudinal bar, measured via dial indicators (Fig. 6c), are shown in Fig. 20.

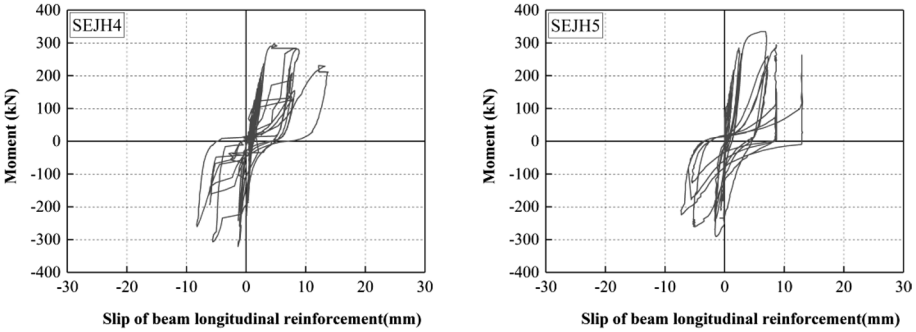


(g) (h)

**Fig. 20** (continued)

The slip of the beam reinforcements of the specimen EJN1 was smaller than that of the specimens EJH1 and EJH2. It showed that the increase of reinforcement strength could enhance the slip of reinforcements in the section through the joint. Compared with the specimens EJH1 and EJH2, the slip amount of the specimens SEJH1 and SEJH2 were smaller, which indicated that the HSSFRC was more excellent than the HSC in reduction the slip of the beam reinforcements when coupled with the HSS bars. And the slippage of specimens SEJH3-SEJH5 reinforced with HSSFRC in the core area or beam end was smaller than that of EJH2. Therefore, HSSFRC had a positive influence on the slip of beam reinforcements through the joint section.

## 4 Prediction of failure mode and strength

The design shear strength of BCJs and the shear force when the beam reached the peak load was compared to predict the failure modes. GB 50010-2010 (2010) specifies that the shear strength formula of joints, $V_{c,GB}$, is as follows:

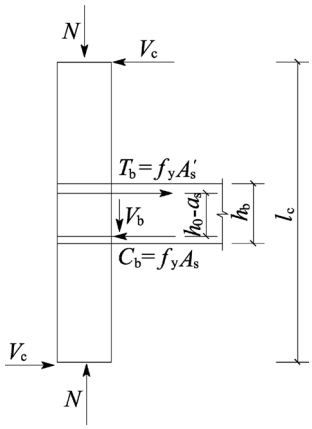


**Fig. 21** Force distribution of BCJs

$$V_{c,GB} \le 1.1\eta_j f_t b_j h_j + f_{yv} A_{svj} \frac{h_{b0} - a'_s}{s} + 0.05\eta_j N \frac{b_j}{b_c} \tag{6}$$

where $\eta_j$ is the constraint influence coefficient of orthogonal beams on joints; $f_t$ is the tensile strength of concrete; $h_j$ and $b_j$ are the height and width of the joint; $f_{yv}$ is the yield strength of stirrup; $h_{b0}$ is the effective height of the beam; $A_{svj}$ is the sum cross section area of each stirrup in the same calculation direction within the effective calculation width; $N$ is the axial force; and $b_c$ is the width of column section.

Figure 21 presents the force distribution of BCJs. Considering the equilibrium condition, the relationship between the column shear force and the beam shear force can be calculated by Eq. (7):

$$V_b = \frac{V_c l_b}{l_c} \tag{7}$$

where $l_c$ and $l_b$ are the clear spans of the column and beam, respectively; $V_c$ and $V_b$ are the shear force of the column and beam, respectively.

The horizontal shear force, $V_{jh}$, is calculated by the following equation according to the equilibrium condition.

$$f_y A_s (h_{b0} - a'_s) + f_y A'_s (h_{b0} - a'_s) + V_b h_c = V_c l_c \tag{8}$$

$$V_{jh} = f_y A_s + f_y A'_s - V_c \tag{9}$$

where $f_y$ is the yield strength of beam longitudinal reinforcements; $A_s$ and $A'_s$ are the beam longitudinal reinforcement areas under the tension and compression, respectively; $h_c$ is the height of column section.

The shear force, $V_{jh}$, can be calculated by substituting Eqs. (7) and (8) into Eq. (9) as follows:

$$V_{jh} = \frac{\Sigma M_b}{h_{b0} - a'_s} \left(1 - \frac{h_{b0} - a'_s}{H_c - h_b}\right) \tag{10}$$

where $\sum M_b$ is the sum of bending moments at positive and negative loading directions; $h_{b0}$ is the effective height of the beam section; $h_b$ and $H_c$ are the height of beam section

**Table 6** Shear capacity of joints

| Specimens | $V_{jh}$ (kN) | $V_{c,GB}$ (kN) | Failure mode | $V_{jh}/V_{c,GB}$ |
|---|---|---|---|---|
| EJH1 | 979 | 819 | Joint failure | 1.20 |
| EJH2 | 843 | 819 | Joint failure | 1.03 |
| EJN1 | 895 | 819 | Joint failure | 1.09 |
| SEJH1 | 972 | 874 | Joint failure | 1.11 |
| SEJH2 | 911 | 874 | Joint failure | 1.04 |
| SEJH3 | 853 | 845 | Joint failure | 1.01 |
| SEJH4 | 853 | 845 | Joint failure | 1.01 |
| SEJH5 | 853 | 845 | Joint failure | 1.01 |

and column, respectively; and $a'_s$ is the distance from the compression reinforcement to the edge of the compression region.

Table 6 shows the prediction results of failure mode and shear strength of all specimens. $V_{jh}$ is the shear force, calculated by Eq. (10), applied on the BCJs when the beam reached the peak load. The shear strength, $V_{c,GB}$, is calculated by Eq. (6) in accordance with GB 50010-2010. The shear force of the BCJs was higher than the shear strength. Namely, the shear force $V_{jh}$ was 1.01–1.20 times larger than shear strength $V_{c,GB}$. Therefore, the BCJs exhibited shear failure in the joint, which was agreed with the experimental results.

The shear force of specimen EJH1 with 12.4% higher shear compressive ratio was 9.3% higher when compared with specimen EJN1, indicating that shear compressive ratio enhanced the shear capacity significantly. While the shear force of specimen EJH2 with 4% lower shear compressive ratio was 6% lower compared to specimen EJN1. These results showed that reinforcement grade had little effect on the shear capacity. The shear strength of specimens reinforced by HSS bars coupled with HSSFRC was predicted well using GB 50010 code, which had a mean of 1.04 and COV of 4.2%. Moreover, the shear force of specimen SEJH2 was 8% higher than specimen EJH2, which contribute to HSSFRC having positive effect on the shear capacity.

## 5 Conclusion

In this study, eight full-scale exterior BCJs, seven HSSFRC specimens with HSS bars, and one HSC joint with ordinary steel bars were designed and subjected to reversed cyclic loading to evaluate the effect of HSSFRC coupled with HSS bars on the seismic performance. The conclusions are as follows:

Performance of specimens with HSS bars coupled with HSSFRC was found to be satisfactory in terms of improved concrete crushing, enhanced ductility, decreased slippage of beam longitudinal reinforcements due to improved bond degradation between HSS bars and HSSFRC. Specimens with HSS bars exhibited comparable failure modes, secant stiffness and energy dissipation to that with normal-strength steel bars.

Specimens EJN1, EJH1 and EJH2 failed in flexural failure due to bond-slip of beam reinforcements resulting in formation of the plastic hinge and followed by shear failure due to the severe concrete crushing. While SEJH1-SEJH5 showed shear failure in the joint with a little concrete spalling because HSSFRC had a positive effect on crack development and failure mode of joints with HSS bars.

Using HSS bars but with a lower reinforcement amount would increase the peak load of BCJs with identical beam flexural strength as well as enhanced hysteretic hoop area. The development length should be more conservative for BCJs with HSS bars, or it could be controlled if the HSSFRC was incorporated, which would improve the bond condition and prevent bond-slip of HSS bars.

The shear compressive ratio increased the peak load, but HSS bars led to the severest concrete crushing, smallest ductility, and largest beam slippage in joint EJH1. While specimen SEJH1, which had the same shear compressive ratio but increased by HSSFRC, exhibited better failure mode, ductility and energy dissipation.

The shear failure mode in the joint was predicated according to the formulae in accordance with GB 50010 and was agreed with the experimental results. The shear strength of specimens reinforced by HSS bars coupled with HSSFRC was predicted well using GB 50010 code, which had a mean of 1.04 and COV of 4.2%.

According to the experimental results, HSSFRC could induce a certain length of crack development, and it is recommended that an HSSFRC area of at least 1.5 times of effective beam height at the beam end was efficient for reinforcing the area to restrain the slippage of HSS bars and achieve better bonding performance of HSS reinforcements and HSSFRC.

**Funding** This research was financially supported by the National Natural Science Foundation of China (Grant No. 52208160); the Natural Science Foundation of Hebei Province, China (E2021202012) and the Science and Technology Research Project of Higher Education Institutions in Hebei Province, China (CXY2023016).

## Declarations

**Conflict of interest** The authors declare that they have no conflict of interest.

## References

ACI 318-14, American Concrete Institute (2014) Building Code Requirements for Structural Concrete and Commentary. ACI, Farmington Hills

Ahmed A, Saleem MM, Siddiqui ZA (2019) Effect of varying top beam reinforcement anchorage details on ductility of HSC beam-column joints. KSCE J Civ Eng 23(5):2272–2280

Alaee P, Li B (2017a) High-strength concrete exterior beam-column joints with high-yield strength steel reinforcements. Eng Struct 145:305–321

Alaee P, Li B (2017b) High-strength concrete interior beam-column joints with high-yield-strength steel reinforcements. J Struct Eng 143(7):305–321

Alavi-Dehkordi S, Mostofinejad D, Alaee P (2019) Effects of high-strength reinforcing bars and concrete on seismic behavior of RC beam-column joints. Eng Struct 183:702–719

Ashtiani MS, Dhakal RP, Scott AN (2014) Seismic performance of high-strength self-compacting concrete in reinforced concrete beam-column joints. J Struct Eng 140(5):04014002

Chang B, Hutchinson T, Wang X, Englekirk R (2014) Seismic performance of beam-column subassemblies with high-strength steel reinforcement. ACI Struct J 111(6):1329–1338

Chetchotisak P, Arjsri E, Teerawong J (2020) Strut-and-tie model for shear strength prediction of RC exterior beam–column joints under seismic loading. Bull Earthq Eng 18(4):1525–1546

Chun SC, Oh B, Lee SH, Naito CJ (2009) Anchorage strength and behavior of headed bars in exterior beam-column joints. ACI Struct J 106(5):579–590

Dabiri H, Kaviani A, Kheyroddin A (2020) Influence of reinforcement on the performance of non-seismically detailed RC beam-column joints. J Build Eng 31:101333

Dabiri H, Kheyroddin A (2021) An experimental comparison of RC beam-column joints incorporating different splice methods in the beam. Structures 34:1603–1613

Eddy L, Nagai K (2016) Numerical simulation of beam-column knee joints with mechanical anchorages by 3D rigid body spring model. Eng Struct 126:547–558

Ehsani MR, Moussa AE, Vallenilla CR (1987) Comparison of inelastic behavior of reinforced ordinary-and high-strength concrete frames. ACI Struct J 84(2):161–169

Eurocode 8, European Committee for Standardization Eurocode (2004) Design of structures for earthquake resistance. CEN, Brussels

Favvata MJ, Karayannis CG (2014) Influence of pinching effect of exterior joints on the seismic behavior of RC frames. Earthq Struct 6(1):89–110

Feng J, Wang S, Meloni M, Zhang Q, Cai J (2020) Seismic behavior of RC beam column joints with 600 MPa high strength steel bars. Appl Sci 10(13):4684

GB 50011-2010, National Standard of the People's Republic of China (2010) Code for seismic design of buildings. Beijing, China

GB/T 228.1-2010, National Standard of the People's Republic of China (2010) Metallic materials-tensile testing at ambient temperature. Beijing, China

GB/T 50081-2019, National Standard of the People's Republic of China (2019) Standard for test method of mechanical properties on ordinary concrete. Beijing, China

Ghani KDA, Hami NHA (2013) Comparing the seismic performance of beam-column joints with and without SFRC when subjected to cyclic loading. Adv Mater Res 626:85–89
Guan D, Guo Z, Jiang C, Yang S, Yang H (2019) Experimental evaluation of precast concrete beam-column connections with high-strength steel rebars. KSCE J Civ Eng 23(1):238–250
Harajli M, Hamad B, Karam K (2002) Bond-slip response of reinforcing bars embedded in plain and fiber concrete. J Mater Civil Eng 14(6):503–511
Hwang H, Park H, Choi W, Chung L, Kim J (2014) Cyclic loading test for beam-column connections with 600 MPa (87 ksi) beam flexural reinforcing bars. ACI Struct J 111(4):913–924
Kang THK, Kim S, Shin JH, LaFave JM (2019) Seismic behavior of exterior beam-column connections with high-strength materials and steel fibers. ACI Struct J 116(4):31–43
Khan MI, Al-Osta MA, Ahmad S, Rahman MK (2018) Seismic behavior of beam-column joints strengthened with ultra-high performance fiber reinforced concrete. Compos Struct 200:103–119
Kheni D, Scott RH, Deb SK, Dutta A (2015) Ductility enhancement in beam-column connections using hybrid fiber-reinforced concrete. ACI Struct J 112(2):167–178
Kheyroddin A, Rouhi S, Dabiri H (2021) An experimental study on the influence of incorporating lap or forging (GPW) splices on the cyclic performance of RC columns. Eng Struct 241:112434
Kim SW, Chang HJ (2021) Structural performance of reinforced concrete interior beam-column joints with high-strength bars. Arch Civ Mech Eng 21(3):1–14
Kotsovou G, Mouzakis H (2012) Seismic design of RC external beam-column joints. B Earthq Eng 10(2):645–677
Li B, Lam ES, Wu B, Wang YY (2013) Experimental investigation on reinforced concrete interior beam-column joints rehabilitated by ferrocement jackets. Eng Struct 56:897–909
López JÁ, Serna P, Navarro-Gregori J, Coll H (2016) A simplified five-point inverse analysis method to determine the tensile properties of UHPFRC from unnotched four-point bending tests. Compos Part B 91:189–204
Raj SD, Ganesan N, Abraham R (2020) Role of fibers on the performance of geopolymer concrete exterior beam column joints. Adv Concr Constr 9(2):115–123
Rautenberg JM, Pujol S, Tavallali H, Lepage A (2013) Drift capacity of concrete columns reinforced with high-strength steel. ACI Struct J 110(2):307–317
Ríos JD, Leiva C, Ariza MP, Seitl S, Cifuentes H (2019) Analysis of the tensile fracture properties of ultra-high-strength fiber-reinforced concrete with different types of steel fibers by X-ray tomography. Mater Design 165:107582
Saghafi MH, Shariatmadar H (2018) Enhancement of seismic performance of beam-column joint connections using high performance fiber reinforced cementitious composites. Constr Build Mater 180:665–680
Su J, Li Z, Prasad Dhakal R, Li C, Wang F (2021) Comparative study on seismic vulnerability of RC bridge piers reinforced with normal and high-strength steel bars. Struct 29:1562–1581
Tang J, Hu C, Yang K, Yan Y (1992) Seismic behavior and shear strength of framed joint using steel-fiber reinforced concrete. J Struct Eng 118(2):341–358
Tapan M, Comert M, Demir C, Sayan Y, Orakcal K, Ilki A (2013) Failures of structures during the October 23, 2011 Tabanlı (Van) and November 9, 2011 Edremit (Van) earthquakes in Turkey. Eng Fail Anal 34:606–628
Wang DH, Ju YZ, Zheng WZ (2017) Strength of reactive powder concrete beam-column joints reinforced with high-strength (HRB600) bars under seismic loading. Strength Mater 49(1):139–151
Xu BW, Shi HS (2009) Correlations among mechanical properties of steel fiber reinforced concrete. Constr Build Mater 23(12):3468–3474
Zainal SMIS, Hejazi F, Rashid RSM (2021) Enhancing the performance of knee beam-column joint using hybrid fibers reinforced concrete. Int J Concr Struct Mater 15(1):20